J Neurophysiol 90: 1635–1642, 2003.
First published May 21, 2003; 10.1152/jn.00150.2003.

Sodium Currents in Neurons From the Rostroventrolateral Medulla of the Rat

Ilya A. Rybak,[1] Krzysztof Ptak,[2] Natalia A. Shevtsova,[1] and Donald R. McCrimmon[2]
[1]*School of Biomedical Engineering, Science and Health Systems, Drexel University, Philadelphia, Pennsylvania 19104; and* [2]*Department of Physiology and Institute for Neuroscience, Feinberg School of Medicine, Northwestern University, Chicago, Illinois 60611-3008*

Submitted 18 February 2003; accepted in final form 15 May 2003

Rybak, Ilya A., Krzysztof Ptak, Natalia A. Shevtsova, and Donald R. McCrimmon. Sodium currents in neurons from the rostroventrolateral medulla of the rat. *J Neurophysiol* 90: 1635–1642, 2003. First published May 21, 2003; 10.1152/jn.00150.2003. Rapidly inactivating and persistent sodium currents have been characterized in acutely dissociated neurons from the area of rostroventrolateral medulla that included the pre-Bötzinger Complex. As demonstrated in many studies in vitro, this area can generate endogenous rhythmic bursting activity. Experiments were performed on neonate and young rats (P1-15). Neurons were investigated using the whole cell voltage-clamp technique. Standard activation and inactivation protocols were used to characterize the steady-state and kinetic properties of the rapidly inactivating sodium current. Slow depolarizing ramp protocols were used to characterize the noninactivating sodium current. The "window" component of the rapidly inactivating sodium current was calculated using mathematical modeling. The persistent sodium current was revealed by subtraction of the window current from the total noninactivating sodium current. Our results provide evidence of the presence of persistent sodium currents in neurons of the rat rostroventrolateral medulla and determine voltage-gated characteristics of activation and inactivation of rapidly inactivating and persistent sodium channels in these neurons.

INTRODUCTION

The persistent sodium current (I_{NaP}) has been found important for intrinsic pacemaker activity in many types of neurons (e.g., see Alonso and Llinàs 1989; Bevan and Wilson 1999; Dickson et al. 1997; Llinàs et al. 1991; Pape and Driesang 1998; Pennartz et al. 1997; Takakusaki and Kitai 1997), yet usually represents 1–4% of the total sodium current (Crill 1996). This current is expressed together with the "classical," rapidly inactivating (or fast) sodium current (I_{Naf}), has an activation threshold ~10 mV more negative than activation threshold of I_{Naf} and is characterized by a sustained long-lasting activation during depolarization (Crill 1996).

It has been suggested that I_{NaP} plays an essential role in the activation of pacemaker neurons in the pre-Bötzinger Complex (pBC), a region within the rostroventrolateral medulla (RVLM), in vitro (Butera et al. 1999; Del Negro et al. 2001; Smith et al. 2000). Del Negro et al. (2002) experimentally characterized I_{NaP} in pBC neurons. This study, however, focused exclusively on a noninactivating component of sodium current. The authors did not characterize I_{Naf} and hence did not separate I_{NaP} from the total noninactivating sodium current. The objective of our study was to experimentally characterize voltage-gated and kinetic properties of both I_{Naf} and I_{NaP} in the area of RVLM including the pBC. A preliminary report of this work was published in abstract form (Shevtsova et al. 2002).

METHODS

Acutely dissociation procedure

Neurons were dissociated according to techniques described by McCrimmon et al. (2001). Briefly, newborn and young (1–15 days old) Sprague-Dawley rats were anaesthetized using isoflurane and decapitated. Sagittal Vibratome (Series 1000, Vibratome, St Louis, MO) slices of the brain stem (300-μm-thick) were collected in Tyrode's solution containing (in mM) 150 NaCl, 4 KCl, 2 $CaCl_2$, 2 $MgCl_2$, 10 HEPES, and 10 glucose, pH 7.4, 300 ± 5 mosM/l. The slices were incubated for 20 min at 33°C in oxygenated minimum essential medium (MEM; Life Technologies, Grand Island, NY) with (in mM) 10 HEPES, 5 L-cysteine and 0.5 EDTA, pH 7.2 to which 20 U/ml of papain (Worthington, Lakewood, NJ) was added. After enzymatic digestion, slices were washed three times in MEM-HEPES to which 1 mg/ml trypsin inhibitor and 1 mg/ml bovine serum albumin had been added.

Our intention was to study neurons from the region of RVLM that included the area of suggested location of the pBC. This area was defined in the sagittal slices by its characteristic distances from the fluorescent-labeled facial and compact/semicompact ambiguous nuclei. These cranial motoneurons were labeled by subcutaneous injection of Fluoro-Gold (50 mg/kg; Fluorochrome, Denver, CO) after birth (Ptak et al. 2001). While viewing the slices at low magnifications with an inverted microscope and epifluorescent ultraviolet illumination, a small region of the RVLM around the suggested location of the pBC was dissected from the slice and then dissociated mechanically using a series of fire-polished Pasteur pipettes. The cell suspension was centrifuged at 1,000 rpm for 10 min, then resuspended, plated onto 35-mm Petri dishes and placed on the stage of an inverted microscope.

Electrophysiological recordings

Borosilicate pipettes (WPI) were pulled, coated with Silicon elastomer (Sylgard, Dow Corning) and fire-polished. Electrode resistance was 1.5–4 MΩ when filled with internal solution containing (in mM) 130 *N*-methyl-D-glucamine, 10 EGTA, 20 HEPES, 20 CsCl, 2 $MgCl_2$, 12 phosphocreatine, 2 Mg-ATP, 0.7 Na_2GTP, and 0.1 leupeptin, pH 7.2 with $CsOH/H_2SO_4$ (265 ± 5 mosM/l). The rapidly inactivating sodium current was recorded using an external solution consisting of (in mM) 15 NaCl, 110 TEA-Cl, 10 HEPES, 10 CsCl, 1 $MgCl_2$, 2 $BaCl_2$, and 0.3 $CdCl_2$ buffered to pH 7.4 with CsOH (300 ± 5 mosM/l). For measurement of persistent sodium current, the external

Address for reprint requests: I. A. Rybak, School of Biomedical Engineering, Science and Health Systems, Drexel University, Philadelphia, PA 19104 (E-mail: rybak@cbis.ece.drexel.edu).

The costs of publication of this article were defrayed in part by the payment of page charges. The article must therefore be hereby marked "*advertisement*" in accordance with 18 U.S.C. Section 1734 solely to indicate this fact.

solution contained (in mM) 115 NaCl, 45 TEA-Cl, 10 CsCl, 10 HEPES, 1 $MgCl_2$, 2 $BaCl_2$, and 0.3 $CdCl_2$ buffered to pH 7.4 with CsOH (300 ± 5 mosM/l). To avoid enhancing effect of low extracellular [Ca^{2+}] on the persistent sodium current (Su et al. 2001), Ca^{2+} was replaced by the same concentration of Ba^{2+} (Magistretti and Alonso 1999). Leak current was revealed by blocking sodium currents with 300 nM TTX and then subtracted. All reagents were obtained from Sigma (St. Louis, MO).

Data acquisition and analysis

Voltage-clamp recordings were made at room temperature (21–22°C) with an Axopatch 200A amplifier (Axon Instruments). After gigaohm seal formation and cell rupture, series resistance was compensated (80–90%) and monitored periodically. Data were acquired with PCLAMP-6 software, CLAMPEX and CLAMPFIT (Axon Instrument), and analyzed with IgorPro (WaveMetrics).

To characterize steady-state properties of I_{Naf}, the standard activation and inactivation protocols were used (Hille 2001). To investigate the steady-state activation, currents were elicited with step depolarization from a holding potential of −80 mV to the potentials between −65 and +20 mV (using 5-mV steps). The conductance values for I_{Naf} were calculated by applying the extended Ohm's law in the form: $g_{Naf} = I_{Naf}/(V - E_{Na})$, where E_{Na} is the reversal (Nernst) Na^+ potential calculated for the solution used in this protocol, and V is the step potential. Data were normalized and fit to the third-order Boltzmann function $g_{Naf}/g_{Naf\,max} = m^3_{\infty Naf} = \{1 + \exp[-(V - V_{1/2mNaf})/k_{mNaf}]\}^{-3}$, where $m_{\infty Naf}$ is the steady state of activation variable, $V_{1/2mNaf}$ is the half activation voltage, k_{mNaf} is the slope factor.

To investigate the steady-state inactivation, currents elicited by a step depolarization to 20 mV from holding potentials between −115 and −20 mV (100-ms prepulse; 5-mV step). The steady-state inactivation curve was estimated by way of normalizing peak current, plotting the normalized currents versus potentials, and fitting the resultant curve to the first-order Boltzmann function $I/I_{max} = h_{\infty Naf} = \{1 + \exp[(V - V_{1/2hNaf})/k_{hNaf}]\}^{-1}$, where $h_{\infty Naf}$ is the steady state of inactivation variable, $V_{1/2hNaf}$ is the half inactivation voltage, k_{hNaf} is the slope factor.

The activation time constant, $\tau_{mNaf}(V)$, was calculated from the time-to-peak [$t_o(V)$] data in each voltage step (V) during the activation protocol by fitting to first-order exponentials in the form: $I(t, V) = I_{max}(V) \cdot \{1 - \exp[t/\tau_{mNaf}(V)]\}/\{1 - \exp[t_o(V)/\tau_{mNaf}(V)]\}$. To characterize the voltage dependence of the activation time constant, we accepted a formal description in which the maximum value of the time constant corresponded to the half activation voltage (e.g., see Butera et al. 1999). Hence $\tau_{mNaf}(V)$ was fit to the function $\tau_{mNaf}(V) = \bar{\tau}_{mNaf} \cdot \{\cosh[(V - V_{1/2mNaf})/k_{\tau mNaf}]\}^{-1}$, where $V_{1/2mNaf}$ is the half activation voltage, $k_{\tau mNaf}$ is the activation time constant slope factor, and $\bar{\tau}_{mNaf}$ is the maximal value of activation time constant at $V = V_{1/2mNaf}$.

The inactivation time constant, $\tau_{hNaf}(V)$, was evaluated from the data on current decay for each voltage step during the activation protocol by fitting to first-order exponentials in the form: $I(t, V) = [I_i(V) - I_{SS}(V)] \cdot \exp[-(t - t_i)/\tau_{hNaf}(V)] + I_{SS}(V)$, $t \geq t_i$, where $I_i(V)$ is the current value close to $I_{max}(V)$ at the moment t_i, and $I_{SS}(V)$ is the minimal (steady state) value of the decayed current. Similar to the activation time constant, the voltage dependence of inactivation time constant was fit to the function $\tau_{hNaf}(V) = \bar{\tau}_{hNaf} \cdot \{\cosh[(V - V_{1/2hNaf})/k_{\tau hNaf}]\}^{-1}$, where $V_{1/2hNaf}$ is the half inactivation voltage, $k_{\tau hNaf}$ is the inactivation time constant slope factor, and $\bar{\tau}_{\tau hNaf}$ is the maximal value of inactivation time constant at $V = V_{1/2hNaf}$.

The experimentally characterized parameters for activation and inactivation of I_{Naf}, ($V_{1/2mNaf}$, k_{mNaf}, $\bar{\tau}_{mNaf}$, $k_{\tau mNaf}$, $V_{1/2hNaf}$, k_{hNaf}, $\bar{\tau}_{hNaf}$, $k_{\tau hNaf}$) were then incorporated in a computer model (see following text), which was used for simulation of the experimental activation protocol. The maximal conductance $\bar{g}_{Naf}$ was found in computer simulation to match the value of maximal sodium current (I_{max}) in the model to that in the experimental protocol.

To experimentally characterize biophysical properties and voltage-gated characteristics of the I_{NaP}, a slow depolarizing ramp increase of voltage under voltage-clamp conditions is usually applied (e.g., see Magistretti and Alonso 1999; Parri and Crunelli 1998; Taddese and Bean 2002). It is considered that the rapidly inactivating component of sodium current (I_{Naf}) is eliminated under these experimental conditions. However, the problem persists because I_{Naf} has a noninactivating or "window" component resulting from the overlap of its voltage-dependent activation and inactivation characteristics (Baker and Bostock 1997; French et al. 1990; Magistretti and Alonso 1999). The window component (I_{NafW}) is comparable with the I_{NaP} in both the peak magnitude and activation threshold. Similar to the I_{NaP}, the I_{NafW} persists when voltage is slowly increasing. Therefore, the voltage-gated characteristics of I_{NaP}, if obtained without accounting the window current, are likely to characterize a mixture of persistent and window currents. Hence, to characterize a "pure" I_{NaP}, it is necessary to study both I_{Naf} and I_{NaP} in the same neuron and to find a method allowing for separation of the I_{NaP} component from the total noninactivating sodium current. In the present study, we have made an attempt to characterize both fast and persistent sodium currents using a combination of experimental studies and computer modeling.

A slow depolarizing voltage ramp protocol was used to promote inactivation of the rapidly inactivating component of sodium current. The voltage was increased from −80 to 20 mV (at ramps of 100 and 75 mV/s). The evoked current (I_{NaTot}) was considered to consist of the persistent sodium and window currents ($I_{NaTot} = I_{NaP} + I_{NafW}$). The computer model was used to simulate the slow ramp protocol and find the voltage dependence of the window current I_{NafW}. The I_{NaP} was obtained by subtracting the simulated window current from the experimentally measured total current ($I_{NaP} = I_{NaTot} - I_{NafW}$). The conductance value for persistent sodium current was calculated from I_{NaP} by applying the extended Ohm's law in the form: $g_{NaP} = I_{NaP}/(V - E_{Na})$, where E_{Na} is the reversal Na^+ potential calculated for the solution used in this protocol. Data were normalized and fit to the first-order Boltzmann function $g_{NaP}/\bar{g}_{NaP} = m_{\infty NaP} = \{1 + \exp[-(V - V_{1/2mNaP})/k_{mNaP}]\}^{-1}$, where $m_{\infty NaP}$ is the steady state of activation variable, $V_{1/2mNaP}$ is the half activation voltage, k_{mNaP} is the slope factor, and $\bar{g}_{NaP}$ is the maximal conductance of the persistent sodium current.

All average values were expressed as mean ± SD.

Mathematical and computer modeling

The I_{Naf} was described according to the classical Hodgkin-Huxley formalism

$$I_{Naf} = g_{Naf} \cdot (V - E_{Na})$$
$$g_{Naf} = \bar{g}_{Naf} \cdot m^3_{Naf}(V, t) \cdot h_{Naf}(V, t) \quad (1)$$

Activation and inactivation were described by the following differential equations

$$\tau_{mNaf}(V) \cdot \frac{d}{dt} m_{Naf} = m_{\infty Naf}(V) - m_{Naf}$$
$$\tau_{hNaf}(V) \cdot \frac{d}{dt} h_{Naf} = h_{\infty Naf}(V) - h_{Naf} \quad (2)$$

where the steady-state activation and inactivation were described as

$$m_{\infty Naf}(V) = \{1 + \exp[-(V - V_{1/2mNaf})/k_{mNaf}]\}^{-1}$$
$$h_{\infty Naf}(V) = \{1 + \exp[(V - V_{1/2hNaf})/k_{hNaf}]\}^{-1} \quad (3)$$

and the voltage-dependent time constants for activation and inactivation were

$$\tau_{mNaf}(V) = \frac{\bar{\tau}_{mNaf}}{\cosh[(V - V_{1/2mNaf})/k_{\tau mNaf}]}$$

$$\tau_{hNaf}(V) = \frac{\bar{\tau}_{hNaf}}{\cosh[(V - V_{1/2hNaf})/k_{\tau hNaf}]} \quad (4)$$

The I_{NaP} had no inactivation and was described as follows

$$I_{NaP} = g_{NaP} \cdot (V - E_{Na})$$

$$g_{NaP} = \bar{g}_{NaP} \cdot m_{NaP}(V, t)$$

$$\tau_{mNaP}(V) \cdot \frac{d}{dt} m_{NaP} = m_{\infty NaP}(V) - m_{NaP}$$

$$m_{\infty NaP}(V) = \{1 + \exp[-(V - V_{1/2mNaP})/k_{mNaP}]\}^{-1}$$

$$\tau_{mNaP}(V) = \frac{\bar{\tau}_{mNaP}}{\cosh[(V - V_{1/2mNaP})/k_{\tau mNaP}]} \quad (5)$$

All simulations were performed on a Pentium IV computer, 1.7 GHz/512 MB (DELL) with a Windows 2000 operating system using MATLAB 6.0 (MathWorks) ode15s routine for solution of differential equations.

RESULTS

Characterization of the rapidly inactivating sodium current

Figure 1, *A* and *B* illustrates sodium currents in a representative neuron evoked by standard activation and inactivation protocols respectively. Steady-state plots (see Fig. 1*C*) were constructed for this neuron following the subtraction of the TTX-insensitive leak current. Activation data were re-calculated for normalized conductance and fit to the third-order Boltzmann function $m^3_{\infty Naf}$, where $m_{\infty Naf}$ was defined by *Eq. 3* (see METHODS). The first-order Boltzmann function $h_{\infty Naf}$ (see *Eq. 3* in METHODS) was used to fit the inactivation data (Fig. 1*C*).

Nine dissociated neurons were characterized. The average half activation voltage $V_{1/2mNaf} = -43.8 \pm 2.3$ mV and the slope factor $k_{mNaf} = 6.0 \pm 0.8$ mV. The average half inactivation voltage $V_{1/2hNaf} = -67.5 \pm 3.6$ mV and the slope factor $k_{hNaf} = 10.8 \pm 2.4$ mV. Figure 2*A* shows steady-state activation (fit to the 3rd-order Boltzmann function) and inactivation (fit to the 1st-order Boltzmann function) curves for nine neurons studied.

To characterize voltage dependence of time constants for

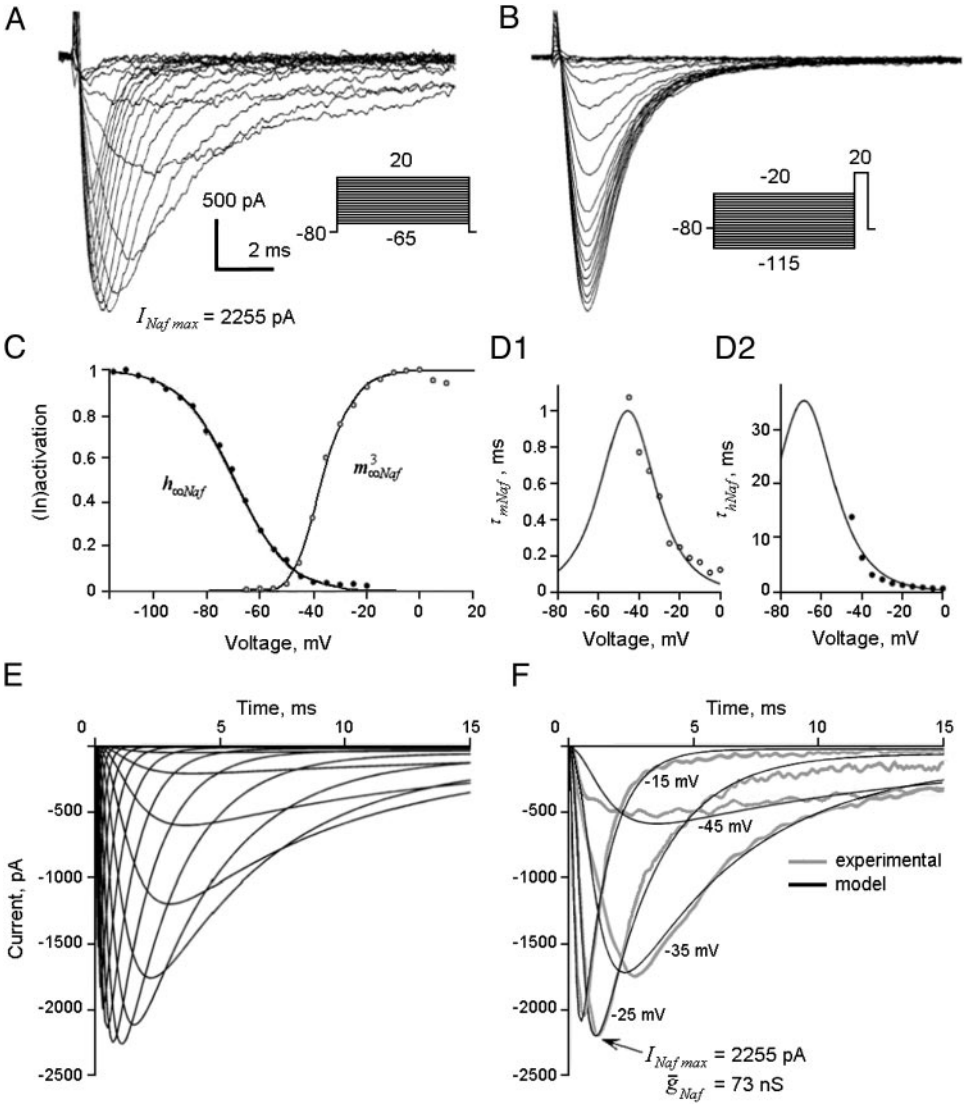

FIG. 1. Activation and inactivation characteristics of rapidly inactivating sodium current. *A* and *B*: current traces in a representative neuron (TTX-subtracted) evoked by protocols used to study the voltage dependence of activation (*A*) and inactivation (*B*). *C*: plots of the voltage dependence of steady-state activation (○) and inactivation (●). The activation data for this neuron fits the 3rd-order Boltzmann function $m^3_{\infty Naf}$ where $m_{\infty Naf}$ is defined by *Eq. 3* (see METHODS) with the half activation voltage $V_{1/2mNaf} = -45.6$ mV and the slope factor $k_{mNaf} = 6.9$ mV. The inactivation data fits the first-order Boltzmann function $h_{\infty Naf}$ (see *Eq. 3* in METHODS) with the half inactivation voltage $V_{1/2hNaf} = -68.4$ mV and the slope factor $k_{hNaf} = 10.1$ mV. *D1* and *D2*: plots of the time constants for activation (○) in *D1*) and inactivation (●) in *D2*) of the same neuron fit to *Eq. 4*, with the maximal value of activation time constant $\bar{\tau}_{mNaf} = 1.0$ ms and $k_{\tau mNaf} = 12.0$ mV (*D1*) and the maximal value of inactivation time constant $\bar{\tau}_{hNaf} = 35.2$ ms and $k_{\tau hNaf} = 12.7$ mV (*D2*). *E*: traces of rapidly inactivating sodium current obtained in simulation of the standard activation protocol. *F*: overlay of the traces for the rapidly inactivating sodium current obtained in simulation at $\bar{g}_{Naf} = 73$ nS and the corresponding experimental traces. The magnitude of $\bar{g}_{Naf} = 73$ was found in simulation to fit the maximal current produced by the voltage step from −80 to −25 mV to the maximal current in the experimental trace corresponding to the same voltage step (pointed by arrow). Overlay of simulated and experimental traces for 3 other steps (from −80 to −15, −35, and −45 mV) are shown as examples.

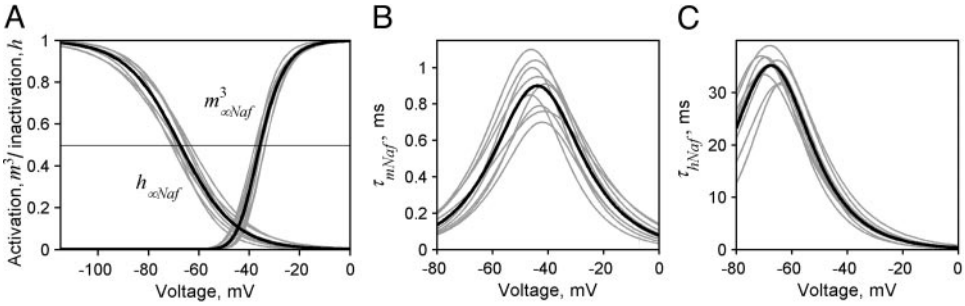

FIG. 2. *A*: plots of the normalized steady-state activation and inactivation of the rapidly inactivating sodium conductance (fit to the 3rd-order Boltzmann function $m^3_{\infty \mathrm{Naf}}$ and the first-order Boltzmann function $h_{\infty \mathrm{Naf}}$, respectively) for 9 neurons studied (grey traces). Black traces show the normalized steady-state activation and inactivation traces corresponding to calculated average values of parameters: $V_{1/2\mathrm{mNaf}} = -43.8$ mV; $k_{\mathrm{mNaf}} = 6.0$ mV; $V_{1/2\mathrm{hNaf}} = -67.5$ mV; $k_{\mathrm{hNaf}} = 10.8$ mV. *B* and *C*: plots of the time constants for activation (*B*) and inactivation (*C*) (fit to *Eq. 4*) for 9 neurons studied (grey traces). Black traces in *B* and *C* show the time constants for activation and inactivation corresponding to the calculated average values of parameters: $\bar{\tau}_{\mathrm{mNaf}} = 0.9$ ms and $k_{\tau\mathrm{mNaf}} = 14.0$ mV (in *B*), and $\bar{\tau}_{\tau\mathrm{hNaf}} = 35.2$ ms and $k_{\tau\mathrm{hNaf}} = 12.8$ mV (in *C*).

fast sodium activation and inactivation, we used the suggestion that these time constants reach their maximal values at the voltages of half activation and half inactivation, respectively. The obtained experimental data were fit to the functions *Eq. 4* (see METHODS). Figure 1, *D1* and *D2* shows examples of voltage dependences of these time constants for the representative neuron. The preceding suggestion and the functions (*Eq. 4*), chosen for the formal description of time constant voltage dependence, provided a good approximation of the experimental data for voltages more positive than −45 mV ($R^2 > 0.95$) (see Fig. 1, *D1* and *D2*). At more negative voltages ($V < -45$ mV), the sodium current was not expressed in our experiments (see Fig. 1*C*). Therefore, for $V < -45$ mV, the type of formal description used to describe the voltage dependence of time constant was not critical for channel kinetics.

Figure 2, *B* and *C*, shows voltage dependences of, respectively, activation and inactivation time constants (fit to the functions *Eq. 4*) for the nine neurons studied. The average value of the maximal activation time constant $\bar{\tau}_{\mathrm{mNaf}} = 0.9 \pm 0.2$ ms and the slope factor $k_{\tau\mathrm{mNaf}} = 14.0 \pm 3.2$ mV. The average value of the maximal inactivation time constant $\bar{\tau}_{\tau\mathrm{hNaf}} = 35.2 \pm 3.4$ ms and $k_{\tau\mathrm{hNaf}} = 12.8 \pm 1.9$ mV.

To define the maximal conductance of rapidly inactivating sodium current ($\bar{g}_{\mathrm{Naf}}$) for each characterized neuron, we ran a computer simulation of the corresponding standard activation protocol. The model was based on *Eqs. 1–4* (see METHODS). In each simulation, the parameters used were taken or drawn from the corresponding experimental measurements for each particular neuron. For example, for the representative neuron in Fig. 1, *A–D*, the following parameter values were used in simulation: $V_{1/2\mathrm{mNaf}} = -45.6$ mV; $k_{\mathrm{mNaf}} = 6.9$ mV; $\bar{\tau}_{\mathrm{mNaf}} = 1.0$ ms; $k_{\tau\mathrm{mNaf}} = 12.0$ mV; $V_{1/2\mathrm{hNaf}} = -68.4$ mV; $k_{\mathrm{hNaf}} = 10.1$ mV; $\bar{\tau}_{\tau\mathrm{hNaf}} = 35.2$ ms; $k_{\tau\mathrm{hNaf}} = 12.7$ mV; $E_{\mathrm{Na}} = 40$ mV. The initial condition for voltage was set to $V(0) = -80$ mV. Voltage steps were applied as follows

$$V(t, n) = -80 + 5 \cdot n \cdot \mathrm{Sgn}(t) \; n = 3, \ldots, 20 \qquad (6)$$

where $\mathrm{Sgn}(x) = \{1, \text{if } x \geq 0;\ 0, \text{otherwise}\}$.

The value of $\bar{g}_{\mathrm{Naf}}$ was found in computer simulation to match the value of maximal sodium current (I_{max}) obtained in the corresponding experimental protocol at the voltage step producing maximal current amplitude. Figure 1*E* shows the results of computer simulation of the standard activation protocol for the representative neuron shown in Fig. 1, *A–D*. For this neuron, the maximal sodium current in the model (at the voltage step from −80 to −25 mV) fit the experimentally defined maximal current of 2,255 pA (revealed at the same voltage step) at $\bar{g}_{\mathrm{Naf}} = 73$ nS (see Fig. 1, *E* and *F*). In nine neurons studied, the maximal conductance for the rapidly inactivating sodium current (defined by the above method) was in the range of $\bar{g}_{\mathrm{Naf}} = 34 - 170$ nS.

Characterization of the persistent sodium current

All of the neurons tested exhibited a non-inactivating, TTX-sensitive sodium current that was evoked by the slow (100 and 75 mV/s) ramp increase of membrane voltage from −80 to 20 mV. Figure 3 shows a noninactivating sodium current (after subtracting the TTX-insensitive component) in the representative neuron (same as in Fig. 1, *A–D*) obtained during the 75-mV/s ramp protocol. This current was activated at about −60 mV and reached a peak near −40 mV (Fig. 3). This total noninactivating current was presumed to consist of the persistent sodium current and the window component of the rapidly inactivating sodium currents: $I_{\mathrm{NaTot}} = I_{\mathrm{NaP}} + I_{\mathrm{NafW}}$.

The voltage-dependent window current for each tested neuron was obtained using computer simulation. The model was used to simulate experimental voltage-ramp protocols. The value of maximal conductance for the rapidly inactivating

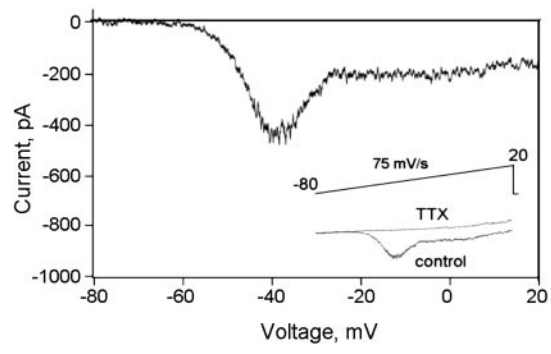

FIG. 3. Non-inactivating sodium current in the representative neuron (same as in Fig. 1, *A–D*) obtained in the 75-mV/s ramp protocol after subtracting the TTX-insensitive component. *Inset:* the control trace for the total current ("control") and the TTX-insensitive current revealed by blocking the TTX-sensitive sodium current by TTX ("TTX").

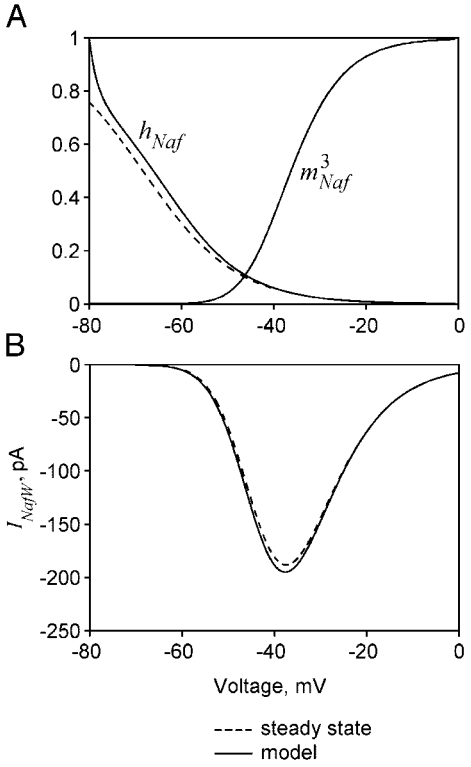

FIG. 4. Examples of matching the voltage-dependent activation and inactivation of the rapidly inactivating sodium conductance (*A*) and the window current (*B*), obtained in simulation of voltage ramp protocol (75 mV/s), to the steady-state traces of these variables. This comparison shows that the transient component of the rapidly inactivating sodium current is almost eliminated, and the remaining window current is close to its steady state.

(fast) sodium current ($\bar{g}_{Naf}$) for each tested neuron was found in advance during simulation of the standard activation protocols. The initial condition for voltage was set to −80 mV [$V(0) = -80$ mV]. The voltage increased with the ramp used in the corresponding experimental protocols ($v = 100$ mV/s = 0.1 mV/ms or 75 mV/s = 0.075 mV/ms)

$$V(t) = -80 + v \cdot t \quad (7)$$

until it reached the value of $V = 20$ mV.

The model was also used to compare the values of parameters of voltage-dependent activation and inactivation for the $I_{Naf}(m^3_{Naf}(V, t)$ and $h_{Naf}(V, t))$ and the value of the window current ($I_{NafW}(V, t) = \bar{g}_{Naf} \cdot m^3_{Naf}(V, t) \cdot h_{Naf}(V, t) \cdot (V - E_{Na})$) obtained in simulations of the ramp voltage protocol with the steady states of these variables ($m^3_{\infty Naf}(V)$, $h_{\infty Naf}(V)$, $I_{\infty NafW} = \bar{g}_{Naf} \cdot m^3_{\infty Naf}(V) \cdot h_{\infty Naf}(V) \cdot (V - E_{Na})$). This comparison demonstrated that both rates of voltage increase used in voltage ramp protocols were sufficient to remove the rapidly inactivating component of sodium current and the remaining window current always reached its steady state. Figure 4 shows an example of this comparison for the representative neuron obtained in simulation of the 75-mV/s voltage ramp protocol.

The persistent sodium current (I_{NaP}) was calculated by subtracting the window current (I_{NafW}) obtained in simulation from the total sodium current (I_{NaTot}) obtained in the ramp voltage protocol

$$I_{NaP} = I_{NaTot} - I_{NafW} \quad (8)$$

Figure 5*A* shows an example of I_{NaTot} and I_{NafW} in the representative neuron, and Fig. 5*B* shows the resultant I_{NaP} for this neuron. The conductance of the persistent sodium current was calculated from I_{NaP} data by applying Ohm's law: $g_{NaP} = I_{NaP}/(V - E_{Na})$. An example for the representative neuron is shown in Fig. 5*C*. The values of conductance were normalized and fit to the first-order Boltzmann function $g_{NaP}/\bar{g}_{NaP} = m_{\infty NaP}$ (see *Eq. 5* in METHODS and an example in Fig. 5, *D* and *E*).

For nine neurons characterized in two voltage ramp protocols, the average half activation voltage for the persistent sodium current and the slope factor were, respectively: $V_{1/2mNaP} = -45.6 \pm 3.1$ mV and $k_{mNaP} = 3.0 \pm 0.4$ mV (for the 100-mV/s protocol) and $V_{1/2mNaP} = -48.6 \pm 3.5$ mV and $k_{mNaP} = 3.2 \pm 0.4$ mV (for the 75-mV/s protocol). Figure 6, *A* and *B*, shows steady-state activation curves (fit to the Boltzmann function) for nine neurons studied in each

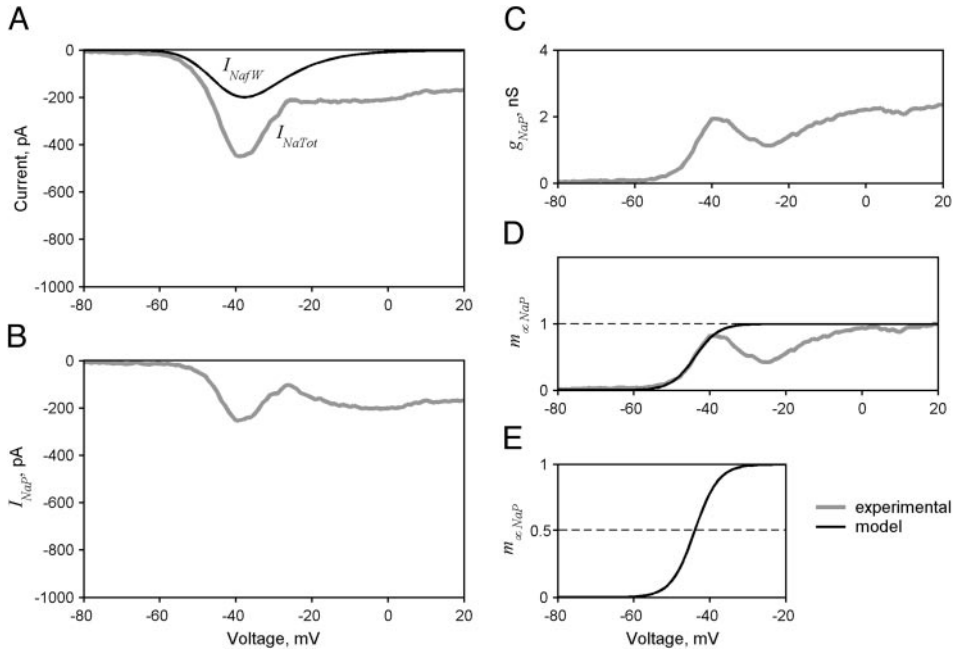

FIG. 5. Characterization of the persistent sodium current in the representative neuron. *A*: superposition of the total noninactivating sodium current (75-mV/s ramp protocol) in the representative neuron (same as in Fig. 1, *A–D*) and the window current obtained in simulation. *B*: the persistent sodium current, I_{NaP}, calculated by subtraction the window current from the total noninactivating sodium current. *C*: the conductance of the persistent sodium current calculated from I_{NaP} by applying Ohm's law. *D* and *E*: the normalized steady-state conductance of the persistent sodium channels in the representative neuron fit to the 1st-order Boltzmann function $m_{\infty NaP}$ with the half activation voltage $V_{1/2mNaP} = -44$ mV and the slope factor $k_{mNaP} = 3.1$ mV.

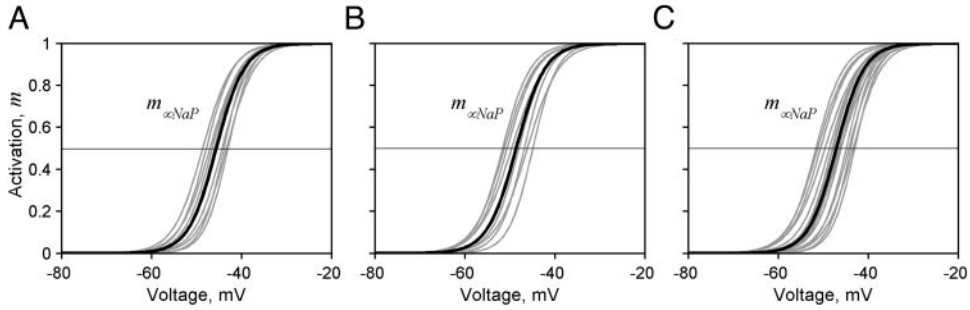

FIG. 6. *A*: plots of the normalized steady-state activation of the persistent sodium conductance (fit to the 1st-order Boltzmann function $m_{\infty NaP}$) for 9 neurons studied, obtained using 100-mV/s ramp protocol (*A*), 75-mV/s ramp protocol (*B*), and both protocols (*C*) (grey traces). Black traces in *A–C* show the normalized steady-state activation corresponding to the calculated average values of parameters: $V_{1/2mNaP} = -45.6$ mV and $k_{mNaP} = 3.0$ mV (in *A*), $V_{1/2mNaP} = -48.6$ mV and $k_{mNaP} = 3.2$ mV (in *B*), and $V_{1/2mNaP} = -47.1$ mV and $k_{mNaP} = 3.1$ mV (in *C*).

ramp protocol. Considering both voltage ramp protocols, the average half activation voltage for persistent sodium current in the characterized neurons $V_{1/2mNaP} = -47.1 \pm 4.1$ mV and the slope factor $k_{mNaP} = 3.1 \pm 0.4$ mV (Fig. 6*C*). The maximal conductance of the persistent sodium channels in nine neurons studied was in the range of $\bar{g}_{NaP} = 0.5 - 5.5$ nS.

To make a backward comparison between the values for I_{NaP} and I_{NaTot} obtained in simulation and those from experimental studies, we ran simulations of the corresponding ramp protocols using the parameters established for the rapidly inactivating and persistent sodium currents in each characterized neuron

$$I_{NaP} = \bar{g}_{NaP} \cdot m_{NaP} \cdot (V - E_{Na})$$

$$I_{NaTot} = I_{Naf} + I_{NaP} = \bar{g}_{Naf} \cdot m_{Naf}^3 \cdot h_{Naf} \cdot (V - E_{Na}) + \bar{g}_{NaP} \cdot m_{NaP} \cdot (V - E_{Na}) \quad (9)$$

$$V(t) = -80 + v \cdot t$$

Examples of matching the experimental and model curves for I_{NaP} and I_{NaTot} for the representative neuron are shown in Fig. 7, *A* and *B*.

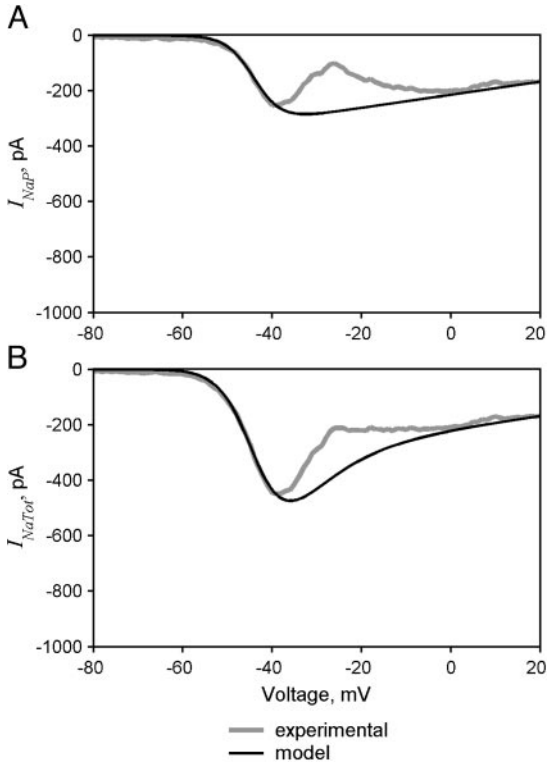

FIG. 7. An example of the backward comparison of values for persistent, I_{NaP} (*A*), and total non-inactivating sodium currents, I_{NaTot} (*B*), obtained in simulation to those from experimental studies.

As seen in Figs. 5*D* and 7, *A* and *B*, the theoretical curves for both the persistent sodium conductance and the current fit well ($R^2 > 0.95$) to the corresponding experimental curves for the initial values of voltage ($V < -35$ mV), where I_{NaP} is activated. They also fit well for the values of voltage beyond the window current ($V > -5$ mV), where the window current is almost completely inactivated and the persistent sodium current is completely activated. This supports the correctness of our estimation of both the voltage-gated characteristics and the maximal conductance of the persistent sodium current. At the same time, there is a significant divergence between the curves within the voltage interval corresponding to inactivation of the window current (see Figs. 5*D* and 7, *A* and *B*). This divergence may slightly diminish the estimated parameters of channel kinetics. It could result from a number of reasons, such as overly simplistic formal description used for both rapidly inactivating and persistent sodium channels, differences in the inactivation of the rapidly inactivating sodium current between the standard and ramp experimental protocols, disregarding the maintained presence of the persistent sodium component during processing data from the standard inactivation protocol. The divergence between the experimental and theoretical curves for persistent sodium current in the range from -35 to -5 mV could also be connected with anomalous properties of I_{NaP} channel noise. Kay et al. (1998) studied steady-state noise characteristics of the persistent sodium conductance experimentally and found that variance of the persistent sodium current is relatively small for voltages less than -40 mV, then dramatically rises in a range from -35 to -25 mV and monotonically decreases for voltages greater than -25 mV. The maximal value of variance in their experiments was in a voltage range from -35 to -5 mV, which corresponds to the largest divergence between the experimental and theoretical curves for persistent sodium current in our study.

DISCUSSION

Some limitations of the present study

The neurons characterized in this study were taken from animals of different ages (P1–P15), and hence possible development-dependent or age-dependent sodium channel expression could influence the variability of our results. Also our studies were performed on acutely dissociated neurons, which retained little of the original axons and dendrites. Therefore characteristics obtained in this study likely relate to somatic and proximal dendritic sodium channels.

In the present study, the maximal conductance of the rapidly inactivating sodium current was determined by matching the simulated and experimental curves corresponding to one step

of the standard activation protocol. Specifically, we used the step that produced maximal current in both simulation and experiment. We did not compare the entire family of curves obtained in simulation with the entire family of experimental curves. A more precise method could be based on the comparison of partial or full families of curves. This idea was not implemented in the present study, but may be used in future investigations.

The present experimental study, including its modeling component, was performed using the assumption that I_{NaP} and I_{Naf} result from the movement of sodium ions through distinct ionic channels. At the same time, it is currently unknown whether these channels are indeed separate or represent different states of uniform but kinetically more complicated sodium channels. This issue is a subject of intense debate (e.g., see Baker and Bostock 1997; Crill 1996; Parri and Crunelli 1998; Taddese and Bean 2002).

Rapidly inactivating sodium channels

This report represents the first attempt to characterize rapidly inactivating sodium currents in RVLM neurons. Analysis of the literature has shown that the steady-state characteristics of voltage-dependent activation and inactivation of I_{Naf} in the RVLM neurons are similar to these in neurons from other regions in the rat brain. Our data also demonstrate that rapidly inactivating sodium current in RVLM neurons has a relatively large window conductance that may produce a window component of the rapidly inactivating sodium current comparable with the persistent sodium current in the same neuron.

Persistent sodium channels

The presence of these channels in RVLM and pBC neurons has been previously reported (Del Negro et al. 2002; Koshiya et al. 2001; McCrimmon et al. 2001; Ptak et al. 2001). Koshiya et al. (2001) reported that the peak conductance of the persistent sodium channels in pBC neurons ranged from 2.4 to 4.5 nS. According to the experimental estimation of Del Negro et al. (2002), this conductance reaches a peak value of 4–5 nS. Our measurements (0.5–5.5 nS) are consistent with these data.

Comparative analysis shows that the half activation voltage for the persistent sodium current in neurons located in different brain areas is usually about or slightly more positive than −50 mV (see Table 1). Our data on the persistent sodium half activation voltage (−47.1 ± 4.1 mV) are reasonably close to this general estimation. Consequently, we assume that the voltage-gated characteristics of the persistent sodium current in the RVLM are similar to those reported for neurons from other brain areas.

Del Negro et al. (2002) reported that the half activation voltage for I_{NaP} in pBC neurons was about −40 mV, which significantly differs from our data for RVLM neurons and data on I_{NaP} in neurons from other brain areas (see Table 1). In contrast to our study, Del Negro et al. (2002) characterized sodium current without considering the contribution of the window component of rapidly inactivating sodium current that, as shown herein, is significant in RVLM neurons. This, however, cannot explain the positive shift in the half activation voltage in their data relative to our results. Also Del Negro et al. (2002) conducted functional identification of neurons before the investigation of I_{NaP} characteristics. They, therefore, could specifically characterize pacemaker neurons in the pBC and separate them from nonpacemaker neurons. We did not perform functional identification of characterized neurons, and hence our data relate to functionally nonidentified RVLM neurons. However, Del Negro et al. (2002) reported a lack of significant difference in voltage-gated characteristics of the I_{NaP} between pacemaker and nonpacemaker neurons. Therefore it is unlikely, that the difference in our data occurred because of the lack of functional identification in our studies. The other difference between the two studies was that we characterized the persistent sodium current in acutely dissociated neurons (and mostly in somatic currents), whereas Del Negro et al. (2002) characterized neurons in slices.

TABLE 1. *Half activation voltage of the persistent sodium channels in neurons from different brain areas*

Source	Brain Area	$V_{1/2mNaP}$, mV
Baker and Bostock (1997)	Dorsal root ganglion (rat)	−49.0*
Brown et al. (1994)	Sensorimotor cortex (rat)	−49.0*
French et al. (1990)	Hippocampus (rat and guinea pig)	−50.0 (in situ and dissociated cells)
Magistretti and Alonso (1999)	Enthorhinal cortex (rat)	−51.3 ± 3.9 (in situ) −48.7 ± 4.7 (dissociated cells)
Parri and Crunelli (1998)	Dorsal root ganglion (rat)	−53.87 ± 3.05
Taddese and Bean (2002)	Hypothalamus (rat)	−54.9*

Parentheses enclose type of animal in second column. Values are means ± SD. * SD is not available.

In summary, results of the present study provide additional evidence of the presence of the persistent sodium current in RVLM neurons. The voltage-dependent characteristics of activation and inactivation of I_{NaP} and I_{Naf} drawn from our experiments may provide a necessary basis for computational modeling and analysis of RVLM neurons.

This work was supported by National Science Foundation Grant 0091942, National Institute of Health (NIH) NS-046062-02 and Office of Naval Research N000140210086 grants to Ilya A. Rybak, and NIH Grants HL-60097, HL-60969, and HL-072415 to Donald R. McCrimmon.

REFERENCES

Alonso A and Llinàs RR. Subthreshold Na^+-dependent theta-like rhythmicity in stellate cells of entorhinal cortex layer II. *Nature* 342: 175–177, 1989.

Baker MD and Bostock H. Low-threshold, persistent sodium current in rat large dorsal root ganglion neurons in culture. *J Neurophysiol* 77: 1503–1513, 1997.

Bevan MD and Wilson CJ. Mechanisms underlying spontaneous oscillation and rhythmic firing in rat subthalamic neurons. *J Neurosci* 19: 7617–7628, 1999.

Brown AM, Schwindt PC, and Crill WE. Different voltage dependence of transient and persistent Na^+ currents is compatible with modal-gating hypothesis for sodium channels. *J Neurophysiol* 71: 2562–2565, 1994.

Butera RJ, Rinzel JR, and Smith JC. Models of respiratory rhythm generation in the pre-Bötzinger Complex. I. Bursting pacemaker neurons. *J Neurophysiol* 82: 382–397, 1999.

Crill WE. Persistent sodium current in mammalian central neurons. *Annu Rev Physiol* 58: 349–362, 1996.

Del Negro CA, Johnson SM, Butera RJ, and Smith JC. Models of respiratory rhythm generation in the pre-Bötzinger Complex. III. Experimental tests of model predictions. *J Neurophysiol* 86: 59–74, 2001.

Del Negro CA, Koshiya N, Butera RJ, and Smith JC. Persistent sodium current, membrane properties and bursting behavior of pre-Bötzinger complex inspiratory neurons in vitro. *J Neurophysiol* 88: 2242–2250, 2002.

Dickson CT, Mena, AR, and Alonso, A. Electroresponsiveness of medial entorhinal cortex layer III neurons in vitro. *Neuroscience* 81: 937–950, 1997.

French CR, Sah P, Buckett KJ, and Gage PW. A voltage-dependent persistent sodium current in mammalian hippocampal neurons. *J Gen Physiol* 95: 1139–1157, 1990.

Hille B. *Ion Channels of Excitable Membranes* (3rd ed.). Sinauer, 2001.

Kay AR, Sigimori M, and Llinàs R. Kinetic and stochastic properties of a persistent sodium current in mature guinea pig cerebellar Purkinje cells. *J Neurophysiol* 80: 1167–1179, 1998.

Koshiya N, Del Negro C, Butera RJ, and Smith JC. Persistent sodium current (INaP) in pre-Bötzinger Complex (pre-BötC) inspiratory neurons. *Soc Neurosci Abstr* 27: 243.3, 2001.

Llinàs RR and Alonso A. Electrophysiology of the mammillary complex in vitro. I. Tuberomammillary and lateral mammillary neurons. *J Neurophysiol* 68: 1307–1320, 1992.

Llinàs RR, Grace AA, and Yarom Y. In vitro neurons in mammalian cortical layer 4 exhibit intrinsic oscillatory activity in the 10- to 50-Hz frequency range. *Proc Natl Acad Sci USA* 88: 897–901, 1991.

Magistretti J and Alonso A. Biophysical properties and slow voltage-dependent inactivation of a sustained sodium current in entorhinal cortex layer-II principal neurons: a whole-cell and single-channel study. *J Gen Physiol* 114: 491–509, 1999.

McCrimmon DR, Monnier A, Ptak K, Zimmo G, Zhang Z, and Alheid GF. Respiratory rhythm generation: PreBötzinger neuron discharge patterns and persistent sodium current. In: *Frontiers in Modeling and Control of Breathing: Integration at Molecular, Cellular and Systems Levels.* New York: Plenum/Kluwer Pub, 2001, p. 147–152.

Pape HC and Driesang RB. Ionic mechanisms of intrinsic oscillations in neurons of the basolateral amygdaloid complex. *J Neurophysiol* 79: 217–226, 1998.

Parri HR and Crunelli V. Sodium current in rat and cat thalamocortical neurons: role of a non-inactivating component in tonic and burst firing. *J Neurosci* 18: 854–867, 1998.

Pennartz CM, Bierlaagh MA, and Geurtsen AM. Cellular mechanisms underlying spontaneous firing in rat suprachiasmatic nucleus: involvement of a slowly inactivating component of sodium current. *J Neurophysiol* 78: 1811–1825, 1997.

Ptak K, Alheid GF, Zhang M, Surmeier DJ, and McCrimmon DR. Characterization of persistent sodium current in the subset of neurons in pre-Bötzinger Complex neurons. *Soc Neurosci Abstr* 27: 633.9, 2001.

Shevtsova NA, Ptak K, McCrimmon DR, and Rybak IA. Study of sodium currents in neurons of pre-Bötzinger complex (pBC). *Soc Neurosci Abstr* 32: 173.5, 2002.

Smith JC, Butera RJ, Koshiya N, Del Negro C, Wilson CG, and Johnson SM. Respiratory rhythm generation in neonatal and adult mammals: the hybrid pacemaker-network model. *Respir Physiol* 122: 131–147, 2000.

Su H, Alroy G, Kirson ED, and Yaari Y. Extracellular calcium modulates persistent sodium current dependent burst-firing in hippocampal pyramidal neurons. *J Neurosci* 21: 4173–8412, 2001.

Taddese A and Bean BP. Subthreshold sodium current from rapidly inactivating sodium channels drives spontaneous firing of tuberomammillary neurons. *Neuron* 33: 587–600, 2002.

Takakusaki K and Kitai ST. Ionic mechanisms involved in the spontaneous firing of tegmental pedunculopontine nucleus neurons of the rat. *Neuroscience* 78: 771–794, 1997.